Research Article

Pulmonary Circulation

Echocardiographic markers of pulmonary hemodynamics and right ventricular hypertrophy in rat models of pulmonary hypertension

Fotios Spyropoulos[1], Sally H. Vitali[2,], Marlin Touma[3], Chase D. Rose[4], Carter R. Petty[5], Philip Levy[4], Stella Kourembanas[4] and Helen Christou[1]

[1]Department of Pediatric Newborn Medicine, Brigham and Women's Hospital, Boston, MA, USA; [2]Department of Anesthesiology, Critical Care and Pain Medicine, Boston Children's Hospital, Boston, MA, USA; [3]University of California at Los Angeles, Los Angeles, CA, USA; [4]Department of Pediatrics, Boston Children's Hospital, Boston, MA, USA; [5]Institutional Centers for Clinical and Translational Research, Boston Children's Hospital, Boston, MA, USA

Abstract

Echocardiography is the gold standard non-invasive technique to diagnose pulmonary hypertension. It is also an important modality used to monitor disease progression and response to treatment in patients with pulmonary hypertension. Surprisingly, only few studies have been conducted to validate and standardize echocardiographic parameters in experimental animal models of pulmonary hypertension. We sought to define cut-off values for both invasive and non-invasive measures of pulmonary hemodynamics and right ventricular hypertrophy that would reliably diagnose pulmonary hypertension in three different rat models. The study was designed in two phases: (1) a *derivation phase* to establish the cut-off values for invasive measures of right ventricular systolic pressure, Fulton's index (right ventricular weight/left ventricle + septum weight), right ventricular to body weight ratio, and non-invasive echocardiographic measures of pulmonary arterial acceleration time, pulmonary arterial acceleration time to ejection time ratio and right ventricular wall thickness in diastole in the hypoxic and monocrotaline rat models of pulmonary hypertension and (2) a *validation phase* to test the performance of the cut-off values in predicting pulmonary hypertension in an independent cohort of rats with Sugen/hypoxia-induced pulmonary hypertension. Our study demonstrates that right ventricular systolic pressure $\geq$35.5 mmHg and Fulton's Index $\geq$0.34 are highly sensitive (>94%) and specific (>91%) cut-offs to distinguish animals with pulmonary hypertension from controls. When pulmonary arterial acceleration time/ejection time and right ventricular wall thickness in diastole were both measured, a result of either pulmonary arterial acceleration time/ejection time $\leq$0.25 or right ventricular wall thickness in diastole $\geq$1.03 mm detected right ventricular systolic pressure $\geq$35.5 mmHg or Fulton's Index $\geq$0.34 with a sensitivity of 88% and specificity of 100%. With properly validated non-invasive echocardiography measures of right ventricular performance in rats that accurately predict invasive measures of pulmonary hemodynamics, future studies can now utilize these markers to test the efficacy of different treatments with preclinical therapeutic modeling.

Keywords

diagnostic techniques and monitoring, echocardiography, pulmonary arterial hypertension, rats, right ventricle function and dysfunction

Date received: 16 December 2019; accepted: 11 February 2020

Pulmonary Circulation 2020; 10(2) 1–10
DOI: 10.1177/2045894020910976

Introduction

Pulmonary hypertension (PH) is a severe and progressive disease characterized by an elevation of pulmonary artery pressure (PAP) and prolonged exposure of the right ventricle (RV) to high afterload.[1–3] Over time, this leads to

The first two authors contributed equally to this manuscript.

Corresponding author:
Fotios Spyropoulos, Department of Pediatric Newborn Medicine, Brigham and Women's Hospital, 75 Francis Street, Thorn 1005, Boston, MA 02115, USA.
Email: fspyropoulos@bwh.harvard.edu

alteration in RV morphology (hypertrophy and dilation), right heart failure, and eventually death if left untreated. Animal models of PH have been commonly utilized to elucidate the pathobiology of this disease with invasive and non-invasive measures of pulmonary hemodynamics and RV performance, and to explore new therapeutic approaches.[4] Interestingly, these techniques are widely used in animal models of PH, but validation and cutoff values of PH have not been established. Therefore, there is a need for highly sensitive and specific non-invasive echocardiographic markers of PH that can be applicable across experimental models allowing us to identify and quantify disease establishment at multiple time-points, as well as monitor the effect of different management strategies.[5]

Characterization of animal models of PH relies on the assessment of hemodynamics by right heart catheterization (RHC) and histopathology from harvested heart and lung tissue. Specifically, RV systolic pressure (RVSP) measured by RHC is traditionally accepted as a surrogate to PAP and serves as the principal diagnostic marker for PH in rats. Fulton's Index (FI) and RV to body weight ratio (RV/BW) allow for assessment of RV hypertrophy by comparing the weights of the RV free wall to the left ventricle (LV) and septal walls and the BW respectively. However, both approaches are terminal procedures that do not allow for longitudinal monitoring and are often cost-prohibitive for establishing the long-term efficacy of the tested interventions. Two-dimensional (2D) echocardiography has the potential to be a noninvasive modality for diagnostic and longitudinal assessments of RV hemodynamics, morphology, and function in experimental animal models. Multiple echocardiographic parameters for assessing RV mechanics have been validated in pediatric and adult PH,[6–10] but only described in animals.[11–14] Examples include measures of RV morphology (end-diastolic RV free wall thickness, RVWTd) and measures of RV afterload (pressure, resistance, and compliance) and indirect measure of RV afterload (pulmonary artery acceleration time (PAAT)). While echocardiography has traditionally been considered to be reliable surrogate for RHC measures and permit serial investigations, it has not been validated with simultaneous echocardiography and RHC for accuracy and reliability in characterization of PH in rats.

We hypothesized that with a properly designed validation study, echocardiographic measurements of RV mechanics in rats can provide reliable estimates of RHC-derived RSVP, FI, and RV/BW. Accordingly, we sought to determine the ability of echocardiography-derived PAAT and RV wall thickness in diastole (RVWTd) to detect elevated RV pressures and hypertrophy in rat models of PH to establish diagnostic echocardiographic thresholds and to validate these diagnostic thresholds in a separate cohort of PH animals.

Materials and methods

Study design

This study consisted of two parts, a derivation phase and a validation phase. In the derivation phase, PH was induced by hypoxic exposure for two weeks or by monocrotaline (MCT) injection (Fig. 1). The rats underwent echocardiography and RHC at the end of the two weeks following hypoxic exposure or after 28 days of the MCT injection. Animals were then sacrificed, and histology was performed. Cut-off values for invasive measures of RV pressure and hypertrophy were determined and non-invasive echocardiography measures of RV morphology and pulmonary hemodynamics were compared against the cut-off values to detect PH. In the validation phase, PH was induced by the combination of Sugen (SU5416) injection and placement in hypoxia for three weeks, a well characterized rat model of PH.[15] After 24 days, the rats underwent echocardiography, RHC, and were then sacrificed for histopathology assessment. Echocardiography derived cut-off values were then determined to accurately predict PH. In both the derivation and validation phases, a normoxia or vehicle-injected

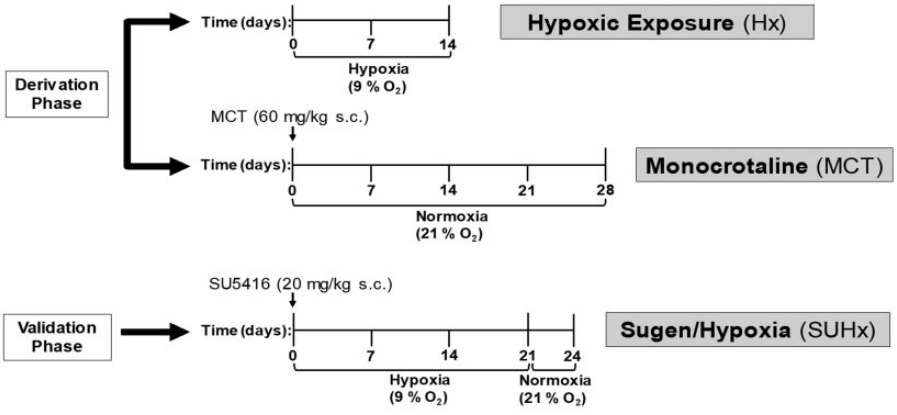

Fig. 1. Schematic of the experimental design.
SU5416: Sugen5416.

control group received echocardiography, underwent RHC, and had histology performed along the same time frames as the three different PH models (Fig. 1).

Animal care and use

All animal experiments were approved by the Brigham and Women's Hospital and Children's Hospital Animal Care and Use Committee and the Harvard Medical Area Standard Committee on Animals.

Adult (12-week-old) male Sprague-Dawley rats (250–400 g) (Charles River Laboratories, Wilmington, MA) were housed in accordance with standard protocols and animal welfare regulations in the animal facility in 12 h/12 h light/dark cycle, at $22 \pm 1^{\circ}C$ ambient temperature and maintained on ad libitum normal Purina Rodent Chow (Purina, St. Louis, MO) and tap water.

Animal models of PH

Hypoxic exposure. Rats were exposed to chronic hypoxia at 9% O_2 inside a plexiglass chamber, where O_2 is controlled to within a 0.2% range by an OxyCycler controller (BioSpherix, Redfield, NY). Electronic controllers injected nitrogen into the hypoxic chamber to maintain the appropriate FiO_2, and ventilation was adjusted to remove CO_2 so that it did not exceed 5000 ppm (0.5%). Ammonia was removed by ventilation and activated charcoal filtration using an electric air purifier. The hypoxic chamber was opened twice a week to replenish food and water and to change the bedding. The duration of hypoxic exposure was two weeks. Control rats were kept in ambient air in the same animal room outside the hypoxic chamber (Fig. 1).

MCT injection. For the MCT model of PH, age-matched rats were given a single subcutaneous injection of 60 mg/kg MCT (Sigma, St. Louis, MO) on day 0. Control rats were injected with the same volume of vehicle (normal saline) and animals were assessed for development of PH 28 days after injection (Fig. 1).

Sugen/hypoxia model. PH was induced in adult (12-week-old) male Sprague-Dawley rats as previously described.[16] The animals were given a single subcutaneously injection of 20 mg/kg of Sugen 5416 (Sigma, St. Louis, MO) in dimethyl sulfoxide (Sigma, St. Louis, MO) and placed in hypoxia for three weeks then returned to normoxia (21% O_2). Oxygen was controlled to $9 \pm 0.2\%$ by an OxyCycler controller (BioSpherix, Redfield, NY). Ventilation was adjusted with a fan and port holes to remove CO_2 and ammonia. The endpoint of the study was 24 days after injection (Fig. 1).

Anesthesia and monitoring

All animals were placed in the supine position for transthoracic echocardiography and RHC and inhaled isoflurane (1–3%) via nosecone was used for anesthesia. Isoflurane was adjusted to maintain heart rates >300 beats per minute.

Transthoracic echocardiography

Transthoracic 2D M-mode and Doppler imaging were performed at the Children's Hospital (derivation phase) and at the Brigham and Women's Hospital Cardiovascular Hemodynamics Core facility (validation phase) using a VisualSonics Vevo 2100 or 3100 ultrasound system respectively and a 20 MHz MicroScan solid-state transducer (Visual Sonics, Toronto, Ontario, Canada). The rats were anesthetized using isoflurane inhalation (1–3%), titrated to a heart rate of 300/min, and were spontaneously breathing during the procedure. Rats' chests were shaved, and fur was removed using depilatory cream.

Pulmonary hemodynamics were assessed through images acquired from a modified left parasternal long-axis view. The pulmonary artery (PA) was visualized using B-mode echocardiography. We used color Doppler to identify an optimal window for PA flow measurements at the level where the medial aspect of the proximal aorta crosses the PA. Subsequently, the pulsed-wave Doppler sample volume was placed in the center of the color Doppler PA. To interrogate PA flow time intervals, PAAT was measured from the interval between the onset of systolic ejection and the peak flow velocity. PA ejection time (ET) was also measured from the interval between the onset of PA ejection to the point of systolic pulmonary arterial flow cessation. To account for heart rate variability, PAAT was adjusted to ET and presented as PAAT/ET. PAAT and ET are non-invasive measure of RV afterload that provide accurate estimates of invasive PVR, PA pressure, and PA compliance in children with PH[17] and in hypoxia PH mouse models.[18]

RV morphology was assessed with end-diastolic RV free wall thickness (RVWTd) by M-mode echocardiography via a modified right parasternal long axis imaging view.[14,19] The ultrasonic beam was placed across the RV wall perpendicular to the RV long axis at the level of the mitral valve.[20]

We assessed RV function using M-mode echocardiography-derived tricuspid annular plane systolic excursion (TAPSE) and measuring the base-to-apex shortening of the RV during systole in the apical four-chamber view.[20]

All measurements were performed off-line by two independent observers in a masked fashion and values were expressed as the mean of measurements taken during 3–5 individual heartbeats. We developed an echocardiography protocol for image acquisition and postprocessing data analysis (Appendix 1).

Cardiac catheterization

All invasive hemodynamic measurements were performed within 24 h of echocardiography using the same anesthetic approach in spontaneously breathing animals. The rats were anesthetized with 2% isoflurane titrated to a heart rate of

300/min and as soon as the level of anesthesia was deemed appropriate, a small transverse incision was made in the abdominal wall, and the transparent diaphragm was exposed. A 23-gauge butterfly needle with tubing attached to a pressure transducer was inserted through the diaphragm and into the RV. The pressure tracing was continuously recorded using PowerLab monitoring hardware and software (ADInstruments, Colorado Springs, CO). Mean RVSP over the first 10 stable heartbeats was recorded, and animals with heart rates less than 300 beats per minute were assumed to be over-anesthetized and were excluded from analysis. All RHC procedures were performed within 24–48 h of echocardiographic examination.

Cardiac tissue processing

Hearts and pulmonary vasculature were perfused in situ with cold 1 × phosphate buffered saline injected into the RV. The heart was excised, and both ventricles were weighed. The RV free wall was then dissected and the remaining LV wall and intraventricular septum (IVS) were weighed. Right ventricular hypertrophy was assessed as FI which is the ratio of RV weight to the LV + IVS weight (RV/LV + IVS) or as the ratio of RV weight to total BW (RV/BW).

Statistical analysis

Cumulative data were analyzed and presented as means ± standard error of the mean. Data analysis was performed using Prism statistical software (Graphpad Software, La Jolla, CA) and STATA 12 (StataCorp. 2011. Stata Statistical Software: Release 12, College Station, TX: StataCorp LP). Multiple group comparisons were done with analysis of variance and Tukey post-test, comparisons of two groups were done with t-test. Significance was defined as $p < 0.05$. Spearman's correlation and linear regression were utilized to analyze correlation between two tests performed in the same animal. Receiver operating characteristic (ROC) curves were plotted to determine optimal cutoff values for invasive and noninvasive tests and areas-under-the-curve (AUC) were calculated. We also determined the intra and inter-rater reliability for each of the measures using intraclass correlation (ICC).

Results

Derivation phase

Development of PH and RV remodeling (Hx, MCT). To investigate the development of PH, RVSP was determined by RHC. Both the hypoxia group and the MCT group had significantly higher RVSP when compared to normoxia controls (42.15 ± 1.98 mmHg, $n = 13$ vs 52.06 ± 3.71 mmHg, $n = 8$ vs 19.65 ± 0.35 mmHg, $n = 8$, respectively $p < 0.0001$, Fig. 2a). Echocardiographic assessment by PAAT/pulmonary artery ejection time (PAET) of PAP inversely correlated with RVSP by RHC ($r = -0.787$, $p < 0.0001$, Fig. 2b). A two-week hypoxic exposure or MCT injection led to a significant

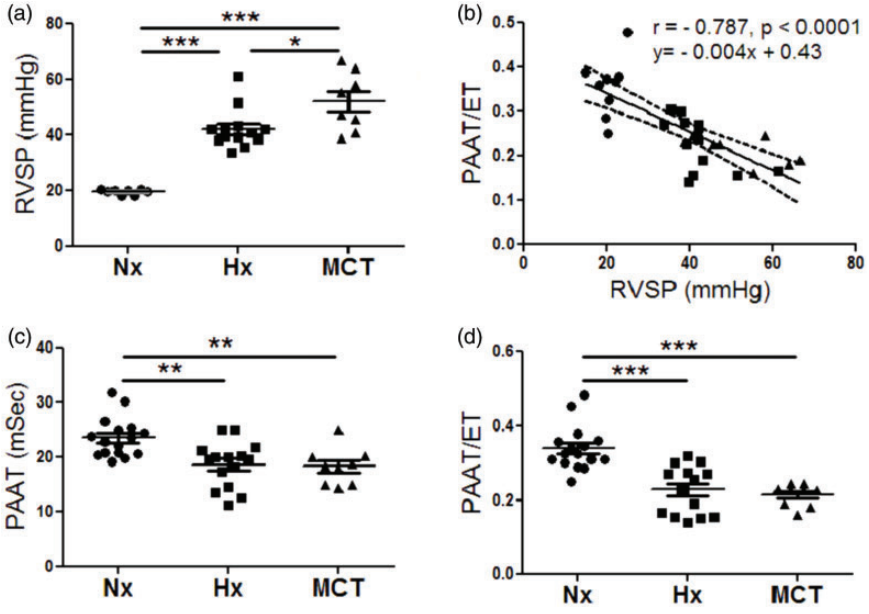

Fig. 2. Derivation phase, development of PH. (a). RVSP measurements for normoxic, hypoxic, and MCT rats, $n = 8$–13 per group. (b) Correlation between PAAT/ET with invasive RVSP ($r = -0.787$, $p < 0.0001$), $n = 30$, dashed lines represent 95% confidence intervals. (c) PAAT for normoxic, hypoxic, and MCT-treated rats, $n = 9$–16 per group. (d) PAAT/ET values for normoxic, hypoxic, and MCT-treated rats, $n = 9$–16 per group. Each data point represents one animal, circles reflect control animals, squares hypoxic, and triangles MCT animals. ***$p < 0.001$ compared to normoxic or vehicle-treated controls, **$p < 0.01$ compared to normoxic or vehicle-treated controls, *$p < 0.05$ between hypoxic and MCT-treated animals. RVSP: right ventricular systolic pressure; PAAT/ET: pulmonary arterial acceleration time/ejection time; Hx: hypoxia; MCT: monocrotaline.

decrease in PAAT and PAAT/ET when compared to normoxic controls (18.71 ± 1.06 msec, $n = 15$, vs 18.35 ± 1.18 msec, $n = 9$, vs 23.6 ± 0.90 msec, $n = 16$, respectively, $p < 0.01$, Fig. 2c), and (0.227 ± 0.016, $n = 15$, vs 0.213 ± 0.009, $n = 9$, vs 0.339 ± 0.015, $n = 16$, respectively, $p < 0.01$, Fig. 2d). Pulmonary hypertensive animals from the hypoxia group and MCT groups both showed the characteristic notched pattern of the pulmonary wave Doppler flow compared to the normoxic controls (Sup Fig. 1a andb).

Morphologically, remodeling of the RV in rats exposed to two weeks of hypoxia and rats that received MCT injection was reflected by significantly increased FI when compared to the normoxia rats (0.46 ± 0.032, $n = 15$, vs 0.48 ± 0.027, $n = 9$ vs 0.21 ± 0.009, $n = 12$, $p < 0.0001$, Fig. 3a). There was a positive correlation of RVWTd thickness derived by M-mode echocardiography to FI ($r = 0.491$, $p = 0.01$, Fig. 3b). RVWTd was also significantly increased in hypoxia-exposed rats compared to normoxic animals (1.189 ± 0.086 mm, $n = 15$, vs. 0.69 ± 0.021 mm, $n = 16$ vs. $p < 0.0001$, Fig. 3c). Similarly, RV/BW ratio was increased in both the hypoxia-exposed rats and the MCT-injected rats (Suppl. Fig. 2a) and correlated with RVWTd ($r = 0.519$, $p = 0.007$, Suppl. Fig. 2b).

Invasive RVSP correlated with measures of RV morphology including FI ($r = 0.784$, $p < 0.0001$, Fig. 3b) and RV/BW ($r = 0.7203$, $p < 0.0001$, data not shown). Similarly, for non-invasive echocardiographic measures, PAAT/ET inversely correlated with both FI ($r = -0.707$, $p < 0.0001$, Fig. 3e) and RV/BW ratio ($r = -0.677$, $p < 0.0001$, Suppl. Fig. 2c). As expected, echocardiographic assessment of RV morphology by RVWTd was also significantly correlated with RVSP ($r = 0.536$, $p = 0.01$, Fig. 3f).

Establishment of cut-off values of invasive and non-invasive measures that predict PH. In order to establish the sensitivity and specificity of echocardiographic measurements for the detection of PH, we first determined the cut-off values for the gold-standard invasive tests of pulmonary hemodynamics (RVSP) and RV hypertrophy (FI and RV/BW). ROC curve analysis showed high sensitivity (97%) and specificity (100%) of RVSP ≥ 35.5 mmHg in distinguishing between controls and animals with hypoxia or MCT-induced PH (AUC = 0.9947, Fig. 4a). Similarly, ROC analysis established that FI ≥ 0.34 or RV/BW ≥ 0.81 mg/g were highly sensitive (94% and 91%, respectively) and specific (97% and 100%, respectively) as cut-off values to distinguish animals with PH (FI (AUC = 0.9877) and RV/BW (AUC = 0.9908), Fig. 4b and c, respectively).

Using the cut-off values for the gold-standard tests established above, we then sought to determine the sensitivity and specificity of the noninvasive measures of PAAT, PAAT/ET, and RVWTd in determining whether an animal developed PH. ROC analysis demonstrated that PAAT ≤ 19 ms was 64% sensitive and 90% specific as a test to detect an

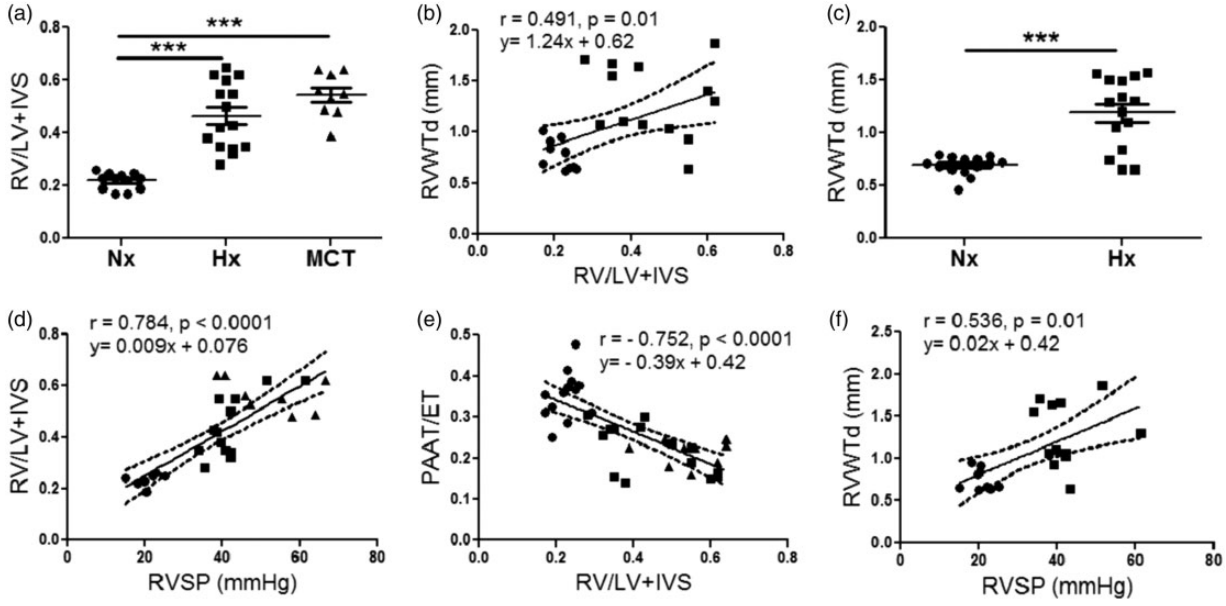

Fig. 3. Derivation phase, correlation of invasive and non-invasive measures of pulmonary hemodynamics (RVSP), and RVH (FI and RV/BW). (a) FI in normoxic, hypoxic, and MCT-treated rats, $n = 9$–15 per group. (b) Correlation between RVWTd and FI ($r = 0.491$, $p = 0.01$), $n = 25$. (c) RVWTd in normoxic and hypoxic, $n = 15$–16 per group. (d) Correlation between FI and RVSP ($r = 0.784$, $p < 0.0001$), $n = 30$. (e) Correlation between PAAT/ET with FI ($r = -0.707$, $p < 0.0001$), $n = 36$. (f) Correlation between RVWTd and RVSP ($r = 0.536$, $p = 0.01$), $n = 21$. Each data point represents one animal, circles reflect control animals, squares hypoxic, and triangles MCT animals. ***$p < 0.001$ compared to normoxic or vehicle-treated controls. Dashed lines represent 95% confidence intervals (b, d–f).

RV: right ventricle; LV: left ventricle; IVS: intraventricular septum; RVWTd: right ventricular wall thickness in diastole; RVSP: right ventricular systolic pressure; PAAT/ET: pulmonary arterial acceleration time/ejection time.

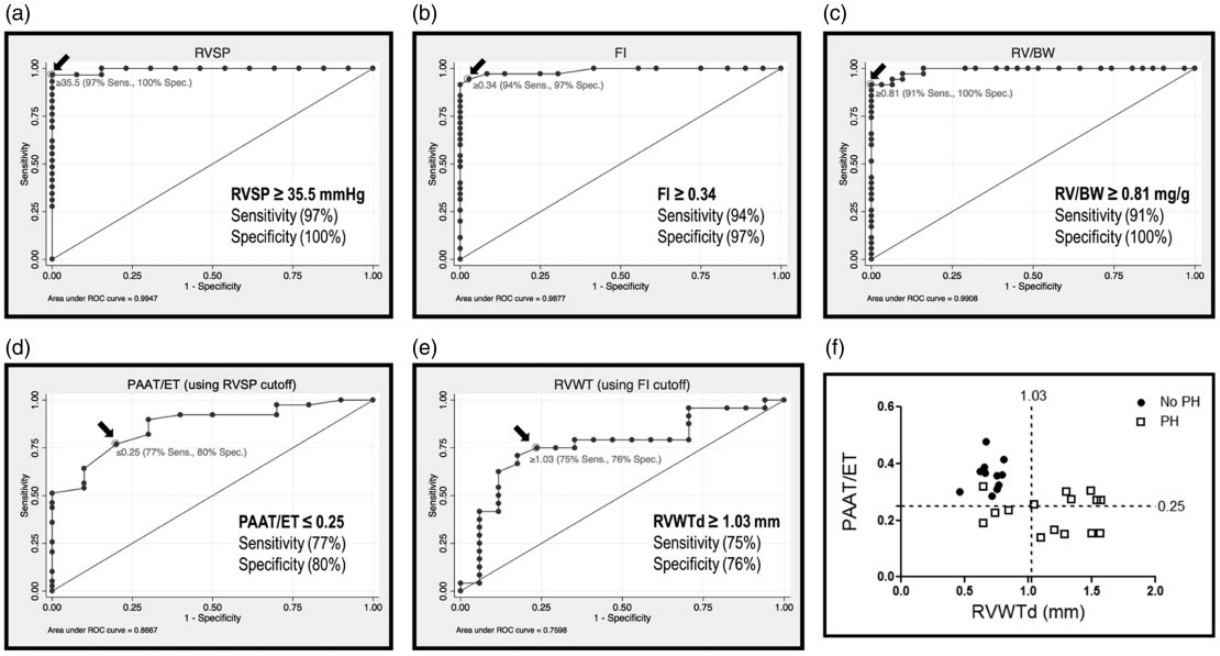

Fig. 4. Invasive and non-invasive measures of pulmonary hemodynamics and RVH predict PH. (a) Receiver operating characteristic (ROC) curve of RVSP. Arrow reflects the cutoff value of ≥35.5 mmHg as distinguishing between normal (normoxic) and pulmonary hypertensive rats with 97% sensitivity and 100% specificity (AUC = 0.9947). (b) ROC curve of Fulton's Index showing the sensitivity and specificity of FI to distinguish between normoxic and PH rats. The cutoff of ≥0.34 distinguishes PH with 94% sensitivity and 97% specificity (AUC = 0.9877). (c) ROC curve showing the sensitivity and specificity of RV/BW to distinguish between normal (normoxic) and PH rats. The cutoff of ≥0.81 mg/g distinguishes pulmonary hypertension with 91% sensitivity and 100% specificity (AUC = 0.9908). (d) ROC curve of PAAT/ET measurement accuracy as an indicator of RVSP ≥ 35.5 mmHg. Cutoff value of ≤0.25 predicts PH with 77% sensitivity and 80% specificity (AUC = 0.8667). (e) ROC curve of RVWTd accuracy in predicting a FI ≥ 0.34. The indicated cutoff value of RVWTd ≥ 1.03 predicts a FI ≥ 0.34 with 75% sensitivity and 76% specificity (AUC = 0.7598). (f) Correlation between PAAT/ET and RVWTd, showing the diagnostic thresholds for PH. Circles reflect animals without PH (RVSP < 35.5 mmHg and/or FI < 0.34), squares represent animals with PH (RVSP ≥ 35.5 mmHg and/or FI ≥ 0.34) (88% sensitivity and 100% specificity when either PAAT/ET ≤ 0.25 and/or RVWTd ≥ 1.03). Each data point represents one animal and dashed lines reflect threshold values.

RVSP: right ventricular systolic pressure; ROC: receiver operating characteristic; FI: Fulton's Index; RV: right ventricle; RV/BW: right ventricle to body weight ratio; PAAT/ET: pulmonary arterial acceleration time/ejection time; RVWTd: right ventricular wall thickness in diastole.

RVSP ≥ the threshold value of 35.5 mmHg (AUC = 0.6885, Suppl. Fig. 2d). A PAAT/ET ratio of ≤ 0.25 detected an RVSP ≥ 35.5 with sensitivity of 77% and a specificity of 80% (AUC = 0.8667, Fig. 4d). Similarly, ROC analysis determined that RVWTd ≥ 1.03 mm was 75% sensitive and 76% specific for determining that an animal developed a FI ≥ the cutoff value of 0.34 (AUC = 0.7598, Fig. 4e) and 68% sensitive and 72% specific for an RV/BW ratio greater than the cutoff value of 0.81 mg/g. (AUC = 0.7197, Sup Fig. 2e). Measuring both PAAT/ET and RVWTd for each animal improved sensitivity and specificity for determining PH. When both echocardiographic measurements were determined, having either a PAAT/ET ≤ 0.25 or a RVWTd ≥ 1.03 mm detected invasively-determined PH with a specificity of 100% and a sensitivity of 88% (Fig. 4f).

The noninvasive echocardiographic index of RV shortening, TAPSE, was measured in a sub set of controls and hypoxic rats (Suppl. Fig. 1e and f). As expected, TAPSE was significantly reduced in the hypoxia group (Suppl. Fig. 3a) compared to controls.

Validation phase

Development of PH and RV remodeling (SUHx). To independently validate the invasive and non-invasive cut-off values of PH established in the derivation phase, we tested our measures in the validation phase with a separate cohort of animals with PH induced by the combination of Sugen and hypoxia for three weeks (Sugen/hypoxia (SUHx)) as described above. We compared this cohort to a group of normoxic animals and sought to define the performance of our measures in predicting PH. As expected, the SUHx animals developed a significant PH phenotype determined by significantly higher RVSP when compared to normoxic controls (50.49 ± 2.71 mmHg, $n = 12$ vs 22.03 ± 1.15 mmHg, $n = 8$, $p < 0.0001$, Fig. 5a). As expected, non-invasive assessment of pulmonary hemodynamics by PAAT/ET inversely correlated with RVSP by RHC ($r = -0.686$, $p < 0.001$, Fig. 5b). Rats in the SUHx group had significantly lower PAAT and PAAT/ET when compared to normoxic controls (20.00 ± 0.85 msec, $n = 11$, vs 26.42 ± 1.25 msec, $n = 12$,

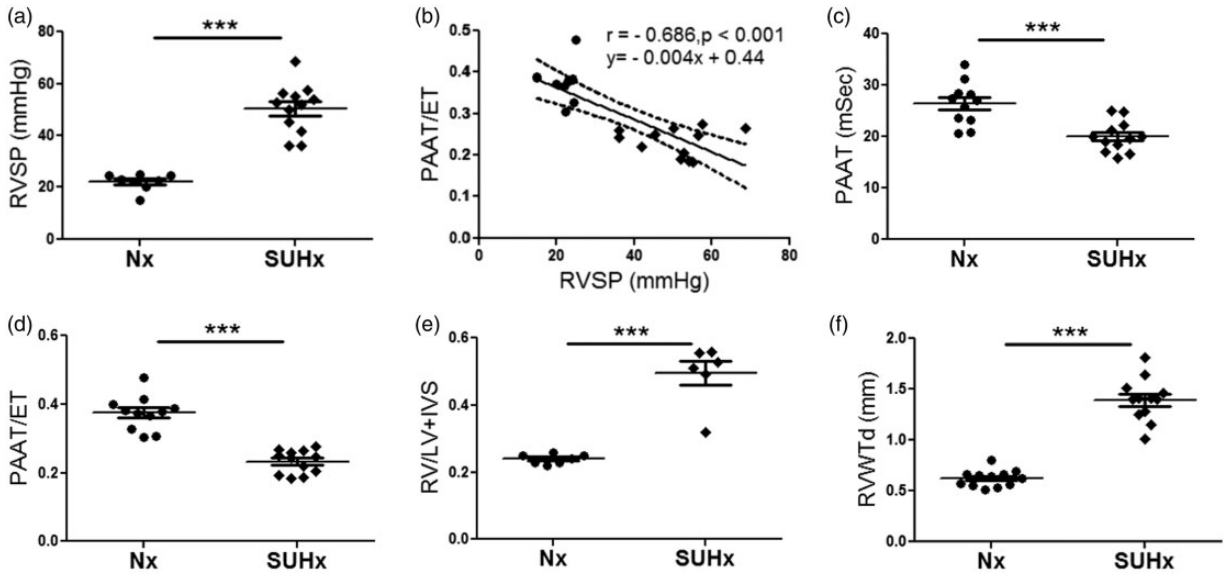

Fig. 5. Validation phase, development of PH, and RV hypertrophy by SUHx. (a) RVSP measurements for normoxic and SUHx rats, $n = 6$–12 animals per group. (b) Correlation between PAAT/ET and invasive RVSP ($r = -0.686$, $p < 0.001$), $n = 20$, dashed lines represent 95% confidence intervals. (c) PAAT, (d) PAAT/ET, (e) FI, and (f) RVWTd for normoxic and SUHx rats, $n = 6$–12 animals per group. Each data point represents one animal, circles reflect control animals, and diamonds SUHx animals. ***$p < 0.0001$ compared to controls.
RVSP: right ventricular systolic pressure; SUHx: Sugen/hypoxia; PAAT/ET: pulmonary arterial acceleration time/ejection time; RV: right ventricle; LV: left ventricle; IVS: intraventricular septum; RVWTd: right ventricular wall thickness in diastole.

respectively, $p < 0.001$, Fig. 5c) and (0.232 ± 0.017 vs. 0.374 ± 0.015, $n = 11$, $n = 12$, respectively, $p < 0.0001$, respectively, Fig. 5d).

We then assessed RV hypertrophy in the SUHx rats and observed a significant increase in the FI compared to control rats (0.49 ± 0.036, $n = 6$, vs 0.24 ± 0.005, $n = 7$, $p < 0.0001$, Fig. 5e). We found a similar significant difference with and RV/BW (data not shown). Echocardiographic assessment of RVWTd was also significantly increased compared to control animals (1.394 ± 0.06 mm, $n = 12$, vs. 0.62 ± 0.023 mm, $n = 12$, $p < 0.0001$, Fig. 5f).

There was a significant inverse correlation between PAAT/ET and FI ($r = -0.754$, $p < 0.005$, Fig. 6a) and RV/BW ratio ($r = -0.809$, $p < 0.005$, Fig. 6b). Similarly, RVWTd was also significantly correlated with RVSP ($r = 0.806$, $p < 0.0001$, Fig. 6c), FI ($r = 0.854$, $p < 0.0005$, Fig. 6d) and RV/BW ratio ($r = 0.844$, $p < 0.001$, Fig. 6e).

Validation of cut-off values established in derivation cohort. In the validation phase, we also generated ROC curves (Suppl. Fig. 4a andb) and tested the performance of the previously derived echocardiographic thresholds. A PAAT/ET ratio ≤ 0.25 was 67% sensitive and 100% specific for determining that an animal had PH. An RVWTd ≥ 1.03 mm was 92% sensitive and 100% specific in identifying animals with PH. When at least one of the cutoffs for PAAT/ET and RVWTd was satisfied to detect invasive measures of PH in the SU/Hx model, the sensitivity and specificity increased to 97% and 100% respectively (Fig. 6f). TAPSE was significantly lower in the SUHx model compared to normoxic controls (Suppl. Fig. 3b).

We obtained clear images in all study echocardiograms and the parameters of PAAT, PAET, RVWTd, and TAPSE were measured. Two independent observers analyzed the echocardiographic data in both cohorts. Inter-rater reliability in the derivation phase and both intra- and inter-rater reliability in the validation phase for all measures are listed in Table 1.

Discussion

This study presents echocardiography-derived thresholds of PAAT, PAAT/ET, and RVWTd as reliable measures of pulmonary hemodynamics and RV morphology. We define quantitative relationships between PAAT/ET and RHC-derived RVSP and RVWTd and FI and show that (1) PAAT/ET and RVWTd are feasible and reproducible in rat models of PH, (2) PAAT/ET inversely correlates with RHC-derived RVSP and RVWTd directly correlates with FI, and (3) a combined PAAT/ET ≤ 0.25 and/or RVWTd ≥ 1.03 mm reliably detect elevated pulmonary pressures and RV hypertrophy in three different rat models of PH.

There is no consensus on which rat model of PH most closely mimics the PH observed in humans. In this study, we employed the three most commonly used rat models to account for all different types of PH. (1) Hypoxia; (2) MCT-induced PH; and (3) SUHx; a more severe and progressive PH model.[15] Several different studies have demonstrated in rat models of SUHx and MCT-induced PH that echocardiography measures of PAAT, TAPSE, and RVWTd matched the corresponding invasive hemodynamic and heart histopathologic data. However, none of the

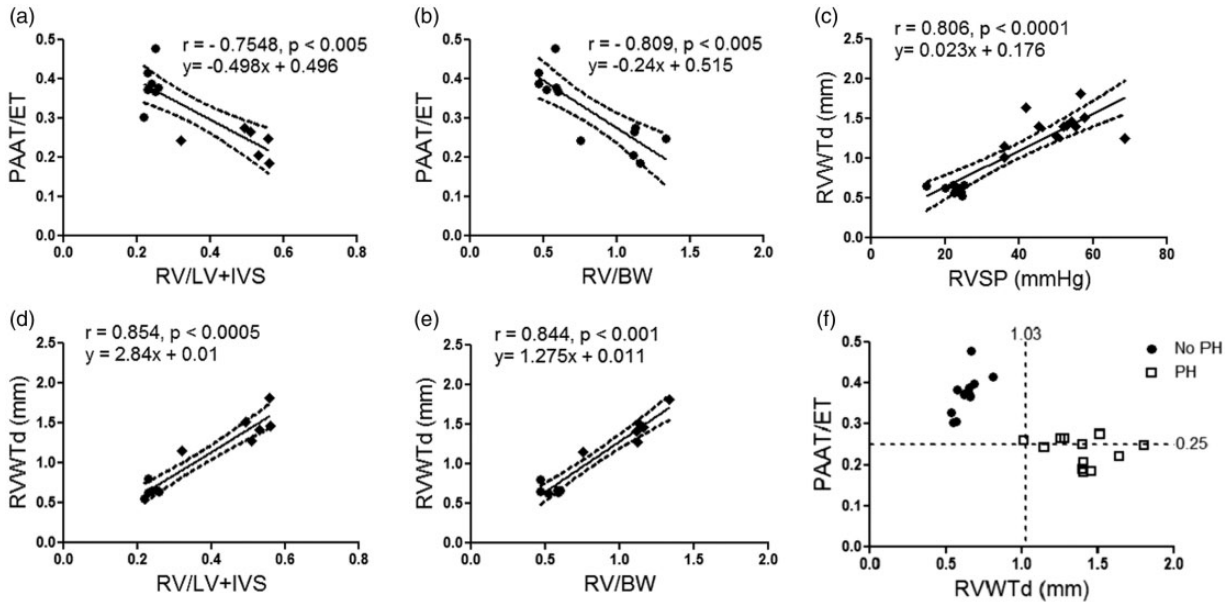

Fig. 6. Echocardiographic measures of PAAT/ET and RVWTd correlate with invasive measures of pulmonary hemodynamics (RVSP), and RVH (FI and RV/BW) in the validation cohort. Correlation between PAAT/ET with (a) FI ($r = -0.7548$, $p < 0.005$), $n = 6$–7 per group; (b) RV/BW ($r = -0.809$, $p < 0.005$), $n = 6$–7 per group. Correlation between RVWTd with (c) invasive RVSP ($r = 0.806$, $p < 0.0001$), $n = 8$–12 per group; (d) FI ($r = 0.854$, $p < 0.0005$), $n = 6$–7 per group; (e) RV/BW ($r = 0.844$, $p < 0.001$), $n = 6$–7 per group. Circles reflect control animals, diamonds SUHx animals, and dashed lines represent 95% confidence intervals. (f) Correlation between PAAT/ET and RVWTd, showing the diagnostic thresholds for PH. Circles reflect animals without PH (RVSP < 35.5 mmHg and/or FI < 0.34), squares represent animals with PH (RVSP ≥ 35.5 mmHg and/or FI ≥ 0.34) (97% sensitivity and 100% specificity when either PAAT/ET ≤ 0.25 and/or RVWTd ≥ 1.03). Each data point represents one animal and dashed lines reflect threshold values.

PAAT/ET: pulmonary arterial acceleration time/ejection time; RV: right ventricle; LV: left ventricle; IVS: intraventricular septum; RV/BW: right ventricle to body weight ratio; RVSP: right ventricular systolic pressure; RVWTd: right ventricular wall thickness in diastole.

Table 1. Echocardiographic reproducibility analysis.

	Derivation phase	Validation phase	
	Interobserver ICC (95% CI), *p*-value	Intraobserver ICC (95% CI), *p*-value	Interobserver ICC (95% CI), *p*-value
RVWTd	0.69 (0.45–0.82), <0.01	0.9801(0.95–0.99), <0.001	0.9825 (0.96–0.99), <0.001
PAAT	0.86 (0.74–0.93), <0.01	0.9376 (0.85–0.97), <0.001	0.8682 (0.7–0.94), <0.001
PAET	0.53 (0.24–0.73), 0.003	0.6052 (0.31–0.84), 0.009	0.7853 (0.54–0.91), 0.007
PAAT/ET	0.90 (0.81–0.95), <0.01	0.8965 (0.76–0.96), <0.001	0.8428 (0.65–0.93), <0.001

RVWTd: right ventricular wall thickness in diastole; PAAT: pulmonary artery acceleration time; PAET: pulmonary artery ejection time.

previous studies have validated these echocardiography measures against invasive cut-off values that detect PH in rat models.[20–24]

In patients with PH, PAAT and PAAT/ET have been shown to be tricuspid regurgitation jet velocity (TRJV)-independent, reliable measures of pulmonary hemodynamics.[6,7,25] In humans with PH, the TRJV is utilized in clinical practice to estimate PA systolic pressure and RVSP by the modified Bernoulli equation. However, it has recently been shown that TRJV is less sensitive to early, small reductions in PA compliance, and minor increases in PA pressure commonly seen with early evidence of PH and RV dysfunction.[10] In rat models of PH, the quantification of TR is not usually feasible unless there is severe PH with PA pressures over 65 mmHg.[24,26] Therefore, a validated non-invasive measure that comprehensively assesses all components of afterload is needed to assess pulmonary hemodynamics, especially in experimental animal models that do not allow for characterization with the TRJV. PAAT and PAAT/ET are not meant to replace RHC as the standard reference method, but they offer an effective tool in animal models in order to monitor for establishment and progression of PH and response to therapeutic interventions.

Noninvasive assessment of RV wall thickness is challenging because the RV's proximity to the sternum makes the window for visualization of a consistent segment of RV wall very narrow. Nevertheless, we were able to consistently locate a segment of RV wall at the level of the mitral valve that could be measured. In humans, the RV wall thickness can be measured in a short axis view at the level of papillary muscle in the LV, but we have found that in rats, the RV and LV can rarely be visualized together in the same short-axis images. Other investigators have assessed RVWTd and found association with RV weight and pressure, but the range of RVWT has varied widely between these reports.[20–24] Our measurements are consistent with those of Urboniene et al., who used the MCT model and the same strain of rats as in our study.[22] Although the ICC measurements for RVWT reflect strong inter-rater reliability, it is not as strong as the ICC for PAAT and PAAT/ET in the derivation phase. We suspect the difference is likely related to the image clarity and challenge of finding an M-mode image at the appropriate level and orientation where the inner and outer aspects of the RV wall are easily distinguished. In the validation phase, VisualSonics (Vevo 3100 ultrasound system) was utilized to acquire images. With the newer image acquiring technique, there was improved intra- and inter-observer reliability across all echocardiographic measures.

The findings in this study may have important implications for standardization of research in experimental animal studies of PH. While the standard approach to assess development, prevention, or reversal of PH is with a combination of tools that characterize RV pressure by RHC or echocardiography, RV weight by histopathology, and RV function by echocardiography,[27] developing non-invasive tools to identify altered pulmonary hemodynamics and RV performance is needed to comprehensively characterize disease establishment, progression, and to follow the animals at multiple timepoints beyond the diagnostic phase. In rats, invasive RHC and histopathologic studies to determine disease are often terminal, invasive, and require large number of subjects for longitudinal studies. Coupling this with a paucity of validated and robust non-invasive methods to characterize the cardio-pulmonary phenotypes in rat models of PH, we feel that the validated non-invasive indices of pulmonary hemodynamic and RV structural assessment from this study can be applicable for assessment of RV phenotype across different rat models of PH.

The importance of these results should be interpreted within the framework of the inherent limitations in this study. PAAT can be affected by heart rate, RV function, hemodynamic conditions and imaging technique. To address the hemodynamic conditions, we utilized a standard anesthetic approach with inhalation induction and animal preparation to ensure that the rats undergo the echocardiograms with similar heart rates, above 300 bpm. Furthermore, to account for any variability in heart rate, PAAT was indexed to ET. Although PAAT has also been indexed to cardiac cycle length to achieve the same normalization,[12] we found an increased sensitivity and specificity for ratio of PAAT/ET to detect PH with RVSP $\geq$ 35.5 when compared with that for PAAT alone. In a small cohort of animals, we also elected to use TAPSE as a measure of RV function which was decreased across all three rat models of PH, but future work should assess the relationship between other measures of RV function (e.g. fractional area of change and deformation imaging) and PAAT measures. There are additional limitations that may limit generalizability of our findings. All of our studies were performed at sea level, so the impact of altitude was not evaluated. Our studies were performed in animals in the 250–400 g weight range by five trained investigators with low intra- and inter- observer variability, but we recognize that the quality of echocardiographic images may be affected by the animals' size and expertise of the investigator.

In conclusion, our study demonstrates that echocardiographic measures of RV performance and pulmonary hemodynamics correlate with RHC-derived pulmonary hemodynamics and histology and can accurately detect PH in different rat models. These validated noninvasive indices permit the characterization of the evolution of PH in rats. With properly validated non-invasive echocardiography measures of RV performance in rats that precisely detect invasive measures of pulmonary hemodynamics, future studies can now utilize these markers to test the efficacy of different management strategies through preclinical therapeutic modeling.

Contributorship

F.S., S.H.V., M.T., and H.C. conceptualized and designed the study. F.S., S.H.V., M.T., C.D.R., C.R.P., and P.L. performed the experiments and statistical analysis of the data and drafted the initial manuscript. H.C. and S.K. provided oversight of the study design, data analysis and interpretation, and procured funding for the project. All authors, critically reviewed, revised, and approved the final manuscript as submitted.

Acknowledgements

We thank Ronglih Liao, MD, Sudeshna Fisch, PhD, and the Brigham and Women's Hospital Cardiac Muscle Research Laboratory Echocardiography Core for training and guidance on echocardiographic techniques. We also thank Mark Perrella, Souheil El-Chemaly, and Ruggero Spadafora for useful comments.

Conflict of interest

The author(s) declare that there is no conflict of interest.

Funding

This work was supported by grants from The National Heart, Lung, and Blood Institute (HL-116573, HL-55454, HL-85446, and K08HL-077344) and The Eunice Kennedy Shriver National Institute of Child Health and Human Development (T32HD-007466 and T32HD-098061).

ORCID iD

Helen Christou https://orcid.org/0000-0002-1663-9701

Supplemental material

Supplemental material for this article is available online.

References

1. Abman SH, Hansmann G, Archer SL, et al. Pediatric pulmonary hypertension: guidelines from the American Heart Association and American Thoracic Society. *Circulation* 2015; 132: 2037–2099.
2. Bossone E, D'Andrea A, D'Alto M, et al. Echocardiography in pulmonary arterial hypertension: from diagnosis to prognosis. *J Am Soc Echocardiogr* 2013; 26: 1–14.
3. Wright LM, Dwyer N, Celermajer D, et al. Follow-up of pulmonary hypertension with echocardiography. *JACC Cardiovasc Imaging* 2016; 9: 733–746.
4. Stenmark KR, Meyrick B, Galie N, et al. Animal models of pulmonary arterial hypertension: the hope for etiological discovery and pharmacological cure. *Am J Physiol Lung Cell Mol Physiol* 2009; 297: L1013–L1032.
5. Michelakis ED, Wilkins MR and Rabinovitch M. Emerging concepts and translational priorities in pulmonary arterial hypertension. *Circulation* 2008; 118: 1486–1495.
6. Dabestani A, Mahan G, Gardin JM, et al. Evaluation of pulmonary artery pressure and resistance by pulsed Doppler echocardiography. *Am J Cardiol* 1987; 59: 662–668.
7. Isobe M, Yazaki Y, Takaku F, et al. Prediction of pulmonary arterial pressure in adults by pulsed Doppler echocardiography. *Am J Cardiol* 1986; 57: 316–321.
8. Levy PT, El Khuffash A, Woo KV, et al. Right ventricular-pulmonary vascular interactions: an emerging role for pulmonary artery acceleration time by echocardiography in adults and children. *J Am Soc Echocardiogr* 2018; 31: 962–964.
9. Levy PT, Patel MD, Groh G, et al. Pulmonary artery acceleration time provides a reliable estimate of invasive pulmonary hemodynamics in children. *J Am Soc Echocardiogr* 2016; 29: 1056–1065.
10. Yared K, Noseworthy P, Weyman AE, et al. Pulmonary artery acceleration time provides an accurate estimate of systolic pulmonary arterial pressure during transthoracic echocardiography. *J Am Soc Echocardiogr* 2011; 24: 687–692.
11. Crnkovic S, Schmidt A, Egemnazarov B, et al. Functional and molecular factors associated with TAPSE in hypoxic pulmonary hypertension. *Am J Physiol Lung Cell Mol Physiol* 2016; 311: L59–L73.
12. Neilan TG, Jassal DS, Perez-Sanz TM, et al. Tissue Doppler imaging predicts left ventricular dysfunction and mortality in a murine model of cardiac injury. *Eur Heart J* 2006; 27: 1868–1875.
13. Thibault HB, Kurtz B, Raher MJ, et al. Noninvasive assessment of murine pulmonary arterial pressure: validation and application to models of pulmonary hypertension. *Circ Cardiovasc Imaging* 2010; 3: 157–163.
14. Vitali SH, Hansmann G, Rose C, et al. The Sugen 5416/hypoxia mouse model of pulmonary hypertension revisited: long-term follow-up. *Pulm Circ* 2014; 4: 619–629.
15. Abe K, Toba M, Alzoubi A, et al. Formation of plexiform lesions in experimental severe pulmonary arterial hypertension. *Circulation* 2010; 121: 2747–2754.
16. Hudalla H, Michael Z, Christodoulou N, et al. Carbonic anhydrase inhibition ameliorates inflammation and experimental pulmonary hypertension. *Am J Respir Cell Mol Biol* 2019; 61: 512–524.
17. Levy PT, Patel MD, Groh G, et al. Pulmonary artery acceleration time provides a reliable estimate of invasive pulmonary hemodynamics in children. *J Am Soc Echocardiogr* 2016; 29: 1056–1065.
18. Gomez-Arroyo J, Saleem SJ, Mizuno S, et al. A brief overview of mouse models of pulmonary arterial hypertension: problems and prospects. *Am J Physiol Lung Cell Mol Physiol* 2012; 302: L977–L991.
19. Hansmann G, Fernandez-Gonzalez A, Aslam M, et al. Mesenchymal stem cell-mediated reversal of bronchopulmonary dysplasia and associated pulmonary hypertension. *Pulm Circ* 2012; 2: 170–181.
20. Hardziyenka M, Campian ME, De Bruin-Bon HA, et al. Sequence of echocardiographic changes during development of right ventricular failure in rat. *J Am Soc Echocardiogr* 2006; 19: 1272–1279.
21. Zhu Z, Godana D, Li A, et al. Echocardiographic assessment of right ventricular function in experimental pulmonary hypertension. *Pulm Circ* 2019; 9: 2045894019841987.
22. Urboniene D, Haber I, Fang YH, et al. Validation of high-resolution echocardiography and magnetic resonance imaging vs. high-fidelity catheterization in experimental pulmonary hypertension. *Am J Physiol Lung Cell Mol Physiol* 2010; 299: L401–L412.
23. Bonnet P, Bonnet S, Boissiere J, et al. Chronic hypoxia induces nonreversible right ventricle dysfunction and dysplasia in rats. *Am J Physiol Heart Circ Physiol* 2004; 287: H1023–H1028.
24. Koskenvuo JW, Mirsky R, Zhang Y, et al. A comparison of echocardiography to invasive measurement in the evaluation of pulmonary arterial hypertension in a rat model. *Int J Cardiovasc Imaging* 2010; 26: 509–518.
25. Kitabatake A, Inoue M, Asao M, et al. Noninvasive evaluation of pulmonary hypertension by a pulsed Doppler technique. *Circulation* 1983; 68: 302–309.
26. Jones JE, Mendes L, Rudd MA, et al. Serial noninvasive assessment of progressive pulmonary hypertension in a rat model. *Am J Physiol Heart Circ Physiol* 2002; 283: H364–H371.
27. Ma Z and Mao L and Rajagopal S. Hemodynamic characterization of rodent models of pulmonary arterial hypertension. *J Vis Exp* 2016; 110: 53335.